

000 SPIKEPINGPONG: SPIKE VISION-BASED FAST-SLOW 001 PINGPONG ROBOT SYSTEM 002 003 004

005 **Anonymous authors**

006 Paper under double-blind review
007
008
009

ABSTRACT

011 Learning to control high-speed objects in dynamic environments represents a fun-
012 damental challenge in robotics. Table tennis serves as an ideal testbed for advanc-
013 ing robotic capabilities in dynamic environments. This task presents two funda-
014 mental challenges: it requires a high-precision vision system capable of accurately
015 predicting ball trajectories under complex dynamics, and it necessitates intelli-
016 gent control strategies to ensure precise ball striking to target regions. High-speed
017 object manipulation typically demands advanced visual perception hardware ca-
018 pable of capturing rapid motion with exceptional temporal resolution. Drawing
019 inspiration from Kahneman’s dual-system theory, where fast intuitive processing
020 complements slower deliberate reasoning, there exists an opportunity to develop
021 more robust perception architectures that can handle high-speed dynamics while
022 maintaining accuracy. To this end, we present *SpikePingpong*, a novel system that
023 integrates spike-based vision with imitation learning for high-precision robotic ta-
024 ble tennis. We develop a Fast-Slow system architecture where System 1 provides
025 rapid ball detection and preliminary trajectory prediction with millisecond-level
026 responses, while System 2 employs spike-oriented neural calibration for precise
027 hittable position corrections. For strategic ball striking, we introduce Imitation-
028 based Motion Planning And Control Technology, which learns optimal robotic
029 arm striking policies through demonstration-based learning. Experimental results
030 demonstrate that *SpikePingpong* achieves a remarkable 92% success rate for 30
031 cm accuracy zones and 70% in the more challenging 20 cm precision targeting.
032 This work demonstrates the potential of Fast-Slow architectures for advancing
033 robotic capabilities in time-critical manipulation tasks.

034 1 INTRODUCTION

035 Current research in robot learning primarily focuses on manipulation tasks involving static or slow-
036 moving objects (Avigal et al., 2022; Wu et al., 2024; Wang et al., 2024; Luo et al., 2024; Vuong
037 et al., 2024; Shao et al., 2020). While these achievements represent significant progress, they
038 predominantly address scenarios with relatively simple dynamics and predictable object behaviors.
039 However, real-world environments are replete with dynamic scenarios involving high-speed mov-
040 ing objects that demand rapid perception and precise control, from catching falling items (Zhang
041 et al., 2024b) and intercepting projectiles (Natarajan et al., 2024) to navigating through crowded en-
042 vironments (Gao et al., 2023). These high-speed scenarios present fundamentally more challenging
043 problems requiring millisecond-level decision making and robust handling of dynamic uncertainties.

044 Table tennis provides an ideal testbed for developing such capabilities, as it constitutes an optimal
045 paradigm for high-speed robotic interaction while exhibiting exceptional generalizability. This task
046 embodies Moravec’s paradox (Moravec, 1988) in its purest form: what appears as a simple recre-
047 ational activity to humans represents one of the most challenging domains for robotics, demanding
048 the integration of high-speed perception, predictive modeling, and precise motor control. Beyond
049 its apparent simplicity, this task systematically encapsulates the fundamental challenges of dynamic
050 robotics: millisecond-scale perception and prediction, precise manipulation under temporal con-
051 straints, and real-time strategic planning. The core competencies developed, including high-speed
052 object tracking, precision manipulation, and adaptive control, demonstrate direct transferability to
053 industrial automation Deka et al. (2024), medical robotics Wah (2025), and aerospace trajectory
interception systems Baradaran (2025). This inherent scalability positions table tennis as a system-

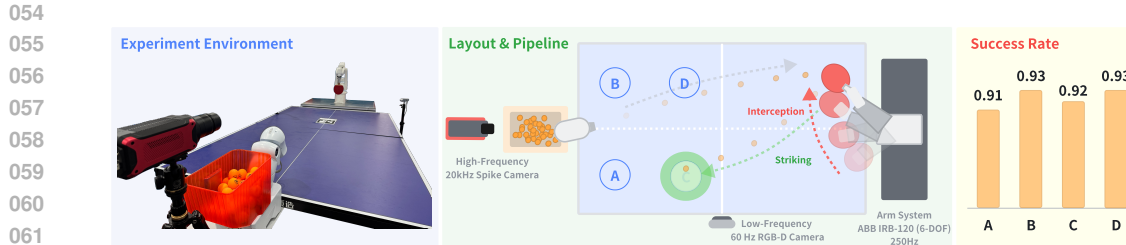


Figure 1: **Overview of SpikePingpong.** Our framework decomposes table tennis into two specialized phases: (1) the interception phase employing a Fast-Slow system architecture to achieve accurate ball interception, and (2) the striking phase utilizing IMPACT, which applies imitation learning to strike the ball to specified target locations. Experimental validation demonstrates 92% success rate for primary accuracy zones and 70% for high-precision targeting across four distinct regions.

atic methodology for developing foundational capabilities essential for advanced robots operating in dynamic, time-critical environments.

When tackling high-speed dynamic tasks like robotic table tennis, existing approaches can be broadly categorized into control-based methods and learning-based methods. Control-based approaches (Acosta et al., 2003; Mülling et al., 2010; Zhang et al., 2018; Silva et al., 2005; Yang et al., 2010) rely on precise physical modeling and predefined motion planning, but despite being mathematically rigorous and computationally efficient, they struggle with real-world complexities due to their requirement for precise calibration and inability to adaptively adjust to varying ball trajectories or unexpected disturbances. Learning-based approaches (Mülling et al., 2013; Abeyruwan et al., 2023; D’Ambrosio et al., 2023; Gao et al., 2020; Ding et al., 2022; Zhao et al., 2024; DAmbrosio et al., 2025; Su et al., 2025), offer greater theoretical adaptability. However, they often suffer from the persistent sim-to-real gap, where policies trained in simulation perform poorly in physical systems. This is particularly pronounced in table tennis, where subtle factors like ball spin and contact dynamics significantly impact performance. Additionally, existing methods typically rely on high-precision hardware vision systems, which are expensive and may still struggle with the rapid temporal dynamics required for accurate trajectory prediction. Drawing inspiration from Kahneman’s dual-system theory (Kahneman, 2011), where fast intuitive processing (System 1) complements slower deliberate reasoning (System 2), there exists an opportunity to develop more robust perception architectures that can handle high-speed dynamics while maintaining accuracy.

To this end, we propose **SpikePingpong**, a high-precision robotic table tennis system integrating spike vision-based Fast-Slow system and advanced control techniques as illustrated in Figure 1. Our system addresses the fundamental challenge of robotic table tennis through a principled decomposition into interception and striking phases, each employing specialized technical innovations. **For the interception phase**, we employ a Fast-Slow system architecture where System 1 provides rapid ball detection and preliminary trajectory prediction with millisecond-level responses, while System 2 leverages high-frequency spike camera data for refined trajectory analysis through neural error correction, effectively addressing physical model inaccuracies caused by environmental variables and spin dynamics. **For the striking phase**, we develop IMPACT (Imitation-based Motion Planning And Control Technology), which learns strategic ball striking through demonstration-based learning, mapping incoming trajectory characteristics to optimal robotic arm striking policies. In summary, our contributions are as follows:

- We design and implement a comprehensive robotic table tennis system that systematically addresses high-speed dynamic manipulation through task-specific decomposition and Fast-Slow architecture.
- We develop a Fast-Slow system perception framework that enables accurate trajectory prediction using conventional cameras through neural error correction, complemented by real-world imitation learning for precise ball striking control.
- We conduct extensive experimental evaluation demonstrating superior performance with 92% success rate in 30cm zones and 70% accuracy in challenging 20cm precision targeting, validating the effectiveness of our integrated approach.

108
109
110
111
112
2 RELATED WORK113
114
115
116
117
118
119
120
121
122
123
124
125
126
127
128
129
130
2.1 AGILE POLICY LEARNING131
132
133
134
135
136
137
138
139
140
141
142
143
144
145
146
147
148
149
150
151
Agile policy learning addresses the challenge of generating fast, adaptive, and robust behaviors in highly dynamic environments. It has been widely studied across various domains such as autonomous driving (Pan et al., 2017; Pomerleau, 1988; Muller et al., 2005; Anzalone et al., 2022; Pan et al., 2020), legged locomotion (Nguyen et al., 2017; Tan et al., 2018; Haarnoja et al., 2018; Zhong et al., 2025), humanoid skills (He et al., 2025; Ben et al., 2025; He et al., 2024; Zhang et al., 2024a), and dynamic manipulation tasks like throwing and catching (Zhang et al., 2024b; Hu et al., 2023; Kim et al., 2014; Huang et al., 2023; Lan et al., 2023). These tasks require policies capable of maintaining high inference frequencies, handling disturbances, and generalizing across a wide range of conditions. Perception plays a critical role in enabling robots to adapt to environmental changes (Wang & Wang, 2022) and to understand the dynamic interaction between objects and agents (Zeng et al., 2020; Kober et al., 2011; Fu et al., 2025). When tracking fast-moving objects, systems often rely on high-speed motion capture setups (Mori et al., 2019). However, in table tennis scenarios, the high speed and abrupt motion of the ball cause significant motion blur with standard RGB cameras, leading to inaccurate position estimates and trajectory predictions. Unlike previous systems that rely on high-precision hardware setups, our *SpikePingpong* system introduces a Fast-Slow system architecture that integrates innovative spike-based vision technology with imitation learning. The Fast system provides rapid ball detection and preliminary trajectory estimation, while the Slow system leverages high-frequency spike camera data for refined trajectory analysis and error correction. This integrated approach compensates for systematic errors without complex physical modeling, significantly improving both interception accuracy and strategic ball striking.152
153
154
155
156
157
158
159
160
161
2.2 ROBOTIC TABLE TENNIS153
154
155
156
157
158
159
160
161
Robotic table tennis has long served as a benchmark task in robotics due to its requirement for real-time perception, prediction, planning, and control. Since Billingsley initiated the first robot table tennis competition in 1983 (Billingsley, 1983), the task has attracted continuous attention from the research community. Existing approaches can be broadly categorized into two groups: control-based methods and learning-based methods. **Control-based approaches** (Acosta et al., 2003; Mülling et al., 2010; Zhang et al., 2018) rely on mathematical modeling and predefined control strategies, typically following a perception-prediction-control pipeline. While these methods benefit from mathematical rigor, they often require precise calibration and struggle with adapting to environmental variations. **Learning-based methods**, particularly reinforcement learning and imitation learning, have gained prominence recently. RL approaches (Büchler et al., 2020; Tebbe et al., 2021; Gao et al., 2020; DAmbrosio et al., 2025; Su et al., 2025) directly map sensory inputs to motor commands, offering greater adaptability. Abeyruwan et al. (Abeyruwan et al., 2023) proposed iterative sim-to-real transfer, while GoalsEye (Ding et al., 2022) employs imitation learning through demonstrations and self-supervised practice, but its sim2real reliance limits performance. Our *SpikePingpong* system differs by introducing a Fast-Slow system perception architecture and real-world imitation learning for ball striking, training directly on data collected from real-world interactions without complex human assistance or simulation dependencies, achieving superior performance and practical deployment.

3 METHOD

153
154
155
156
157
158
159
160
161
In this section, we present our robotic table tennis framework *SpikePingpong*, consisting of two integrated components as shown in Figure 2. Our approach features a Fast-Slow system for perception: System 1 employs physics-based trajectory prediction using an RGB-D camera for rapid ball detection, while System 2 leverages a high-frequency spike camera to refine predictions by compensating for real-world physical effects. For action generation, our Imitation-based Motion Planning And Control Technology module generates strategic hitting motions through imitation learning, enabling tactical control over return placement.

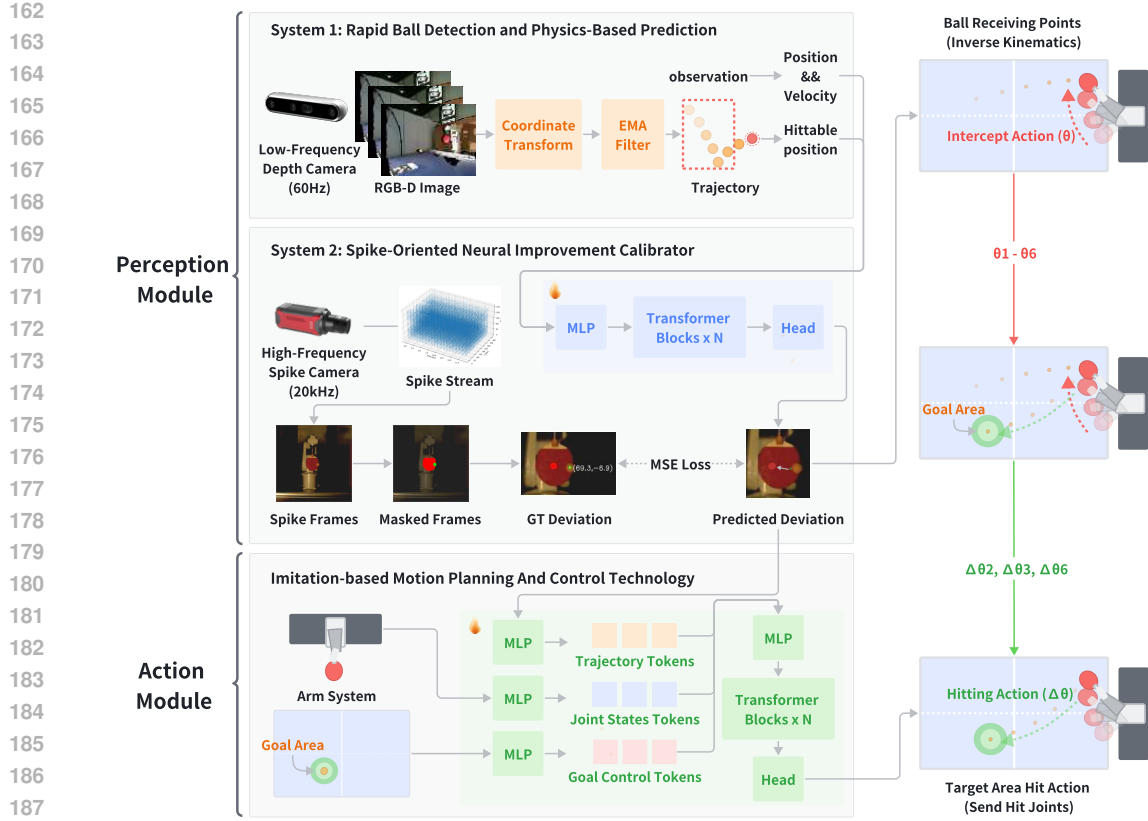


Figure 2: **Framework of SpikePingpong.** Our system integrates two key components: (1) A Fast-Slow system architecture for perception, where System 1 provides rapid trajectory prediction using RGB-D camera data and System 2 serves as a Spike-Oriented Neural Improvement Calibrator for refined hittable position estimation through spike camera data, and (2) IMPACT module for strategic motion planning and control.

3.1 FAST-SLOW SYSTEM BALL INTERCEPTION FRAMEWORK

3.1.1 SYSTEM 1: RAPID BALL DETECTION AND PHYSICS-BASED PREDICTION.

System 1 serves as the foundation of our Fast-Slow system architecture, providing rapid response capabilities for high-speed ball tracking through two core components: real-time ball detection and physics-based trajectory prediction. The detection module extracts ball positions from RGB-D camera streams, while the prediction module utilizes classical physics models to estimate future ball trajectories and determine optimal hittable positions. Additionally, System 1 provides essential contextual information to System 2, including ball state estimates and predicted hittable position that inform the learning-based decision-making process.

Ball Detection. We employ YOLOv4-tiny (bubbliiing, 2020) for its computational efficiency, achieving detection frequencies up to 150 Hz. Our training methodology adopts a two-phase approach: initial pre-training on public datasets (Roboflow (Alexandrova et al., 2015), TT2 (desigproject, 2022), and Ping Pong Detection (pingpong, 2024)), followed by domain-specific fine-tuning. Following object detection, we perform coordinate transformation from image space to world coordinates using calibrated camera parameters, enabling accurate 3D ball position acquisition for subsequent motion planning.

Physics-Based Trajectory Prediction. Our physics-based approach represents another key component of System 1, enabling the system to anticipate the ball’s path and determine optimal hittable positions. The prediction model employs Exponential Moving Average filtering to obtain reliable estimates of the ball’s current position (x, y, z) and velocity (v_x, v_y, v_z). These filtered state estimates

serve as input to our physics model, which outputs the predicted hittable position $(x_{\text{hit}}, y_{\text{hit}}, z_{\text{hit}})$ and corresponding velocity $(v_x^{\text{hit}}, v_y^{\text{hit}}, v_z^{\text{hit}})$. We calculate the time t required for the ball to reach the predetermined hitting plane at y_{hit} : $t = \frac{y_{\text{hit}} - y}{v_y}$. Using this time value, we predict the x-coordinate at the hittable position: $x_{\text{hit}} = x + v_x \cdot t$. If x_{hit} falls outside the robot's operational workspace, the ball is classified as unhittable. For the z-coordinate prediction, we consider two scenarios:

- **Direct trajectory:** If the ball doesn't contact the table before reaching y_{hit} , we compute $z_{\text{hit}} = z + v_z \cdot t + \frac{1}{2}gt^2$. When $z_{\text{hit}} > h_{\text{table}}$, no rebound occurs.

- **Rebound trajectory:** If the ball impacts the table, we calculate the rebound time t_{rb} by solving: $z + v_z \cdot t_{\text{rb}} + \frac{1}{2}gt_{\text{rb}}^2 = h_{\text{table}}$.

We then determine the impact velocity $v_{z,\text{in}}$ and post-rebound velocity $v_{z,\text{out}}$ using:

$$v_{z,\text{in}} = -\sqrt{-2g(z - h_{\text{table}}) + v_z^2}, \quad (1)$$

$$v_{z,\text{out}} = -e \cdot v_{z,\text{in}}. \quad (2)$$

where e represents the coefficient of restitution. The system further evaluates potential secondary rebounds to determine the final z_{hit} and v_z^{hit} .

3.1.2 SYSTEM 2: SPIKE-ORIENTED NEURAL IMPROVEMENT CALIBRATOR

System 2 serves as the learning-based enhancement layer of our Fast-Slow system architecture, addressing the limitations of physics-based predictions through neural calibration. While System 1 provides rapid trajectory estimation under ideal conditions, real-world scenarios introduce deviations due to air resistance, ball spin, and sensor noise that simplified physics models cannot capture. To bridge this gap, System 2 functions as a Spike-Oriented Neural Improvement Calibrator, which learns to predict the systematic discrepancy between System 1's theoretical hittable position and actual optimal interception position. By leveraging high-frequency spike camera observations and contextual information from System 1, System 2 provides precise calibration corrections that significantly enhance overall system accuracy.

Data Collection. System 2 integrates ball trajectory data, velocity measurements, and physics-based predictions to precisely quantify the discrepancy between theoretical and actual hittable positions. For training purposes, we developed an extensive dataset that meticulously documents the systematic variations between physics-model predictions and empirically observed real-world interception positions, enabling our system to learn these complex error patterns.

Specifically, during each trial, we systematically record the ball's 3D position and velocity vectors throughout its trajectory, along with the corresponding hittable position predicted by System 1's physics-based model. Based on these predictions, we compute the required joint angles through inverse kinematics and execute the corresponding robotic arm motion to position the paddle center at the theoretically optimal hittable position. Subsequently, a Spike camera (Dong et al., 2021) captures images of the actual ball-paddle interaction at the moment of contact. The pixel distance between the ball's observed position and the paddle center in these images provides a quantitative measure of the spatial deviation, which serves as the ground truth for System 2.

Network Architecture. System 2's network processes three input modalities: historical position vectors $\mathbf{p}_i \in \mathbb{R}^{K \times 3}$, velocity vectors $\mathbf{v}_i \in \mathbb{R}^{K \times 3}$ from the preceding K frames, and the physics-based predicted hittable position $\mathbf{h}_i \in \mathbb{R}^3$. Each modality is processed through dedicated MLPs with ReLU activation and dropout regularization for feature extraction. The concatenated features are then processed through a Transformer (Vaswani et al., 2017) encoder to capture temporal dependencies and contextual relationships across trajectory segments. Finally, a regression head with fully connected layers maps the refined representation to the predicted deviation vector.

Training Objective. We optimize the model using the mean squared error (MSE) loss function, which minimizes the difference between the predicted and ground-truth deviation vectors:

$$L_{\text{MSE}}(\theta) = \frac{1}{N} \sum_{i=1}^N \|\hat{D}_i - D_i\|^2; \text{ where } \hat{D}_i = f_{\theta}([\mathbf{p}_i, \mathbf{v}_i, \mathbf{h}_i]). \quad (3)$$

270 f_θ represents the neural network with parameters θ , $p_i \in \mathbb{R}^{K \times 3}$ denotes the position history, $v_i \in \mathbb{R}^{K \times 3}$ denotes the velocity history, $h_i \in \mathbb{R}^3$ denotes the expected hittable position, $D_i \in \mathbb{R}^2$ is the ground truth deviation vector, and $\hat{D}_i \in \mathbb{R}^2$ is the predicted deviation vector.
 271
 272
 273

274 Drawing inspiration from dual-system theory in cognitive science (Kahneman, 2011), this Fast-
 275 Slow system architecture combines the speed of immediate heuristic reasoning with the accuracy
 276 of experience-based learning, ensuring both real-time operation and precise task execution. Once
 277 trained, System 2 operates as a lightweight neural predictor that directly estimates deviation vectors
 278 from trajectory features without requiring spike camera feedback during deployment. This design
 279 enables the system to benefit from high-fidelity spike-based training data while maintaining compu-
 280 tational efficiency and real-time performance in operational scenarios.
 281
 282

3.2 IMPACT: IMITATION-BASED MOTION PLANNING AND CONTROL TECHNOLOGY

283 Building upon our Fast-Slow system framework, where System 1 provides rapid physics-based pre-
 284 dictions and System 2 delivers precise neural calibration through spike-oriented improvement, we
 285 introduce **IMPACT** (Imitation-based Motion Planning And Control Technology) for strategic strik-
 286 ing behaviors. This module learns tactical ball-striking through imitation learning, enabling strategic
 287 returns that achieve targeted gameplay beyond mere interception.
 288

289 **Data Collection.** The **IMPACT** module requires high-quality training data that captures the com-
 290 plete striking process from ball trajectory to final landing outcomes. Firstly, we record the incoming
 291 ball trajectory and estimate the optimal hitting position using our Fast-Slow system framework.
 292 Based on this prediction, we compute the corresponding robot joint configurations through inverse
 293 kinematics and position the robotic arm accordingly. To generate diverse striking behaviors, we
 294 apply random angular perturbations to three critical robot joints before executing the stroke. We
 295 retain only successful trials where the ball returns to the opponent’s side, recording the perturbed
 296 joint angles and resulting landing positions. Each sample is labeled according to its specific landing
 297 region for fine-grained strategic control. This approach is highly efficient compared to teleoperation
 298 methods (Takada et al., 2022), as it leverages accurate hitting predictions to automatically position
 299 the robot, significantly reducing collection time while ensuring consistent data quality.
 300

301 **Network Architecture.** The **IMPACT** module employs a transformer-based neural network that
 302 processes three input modalities: ball trajectory sequences, robot joint configurations, and desired
 303 landing region specifications (see Figure 2). Each modality is independently encoded into token rep-
 304 resentations using dedicated multi-layer perceptrons (MLPs). These tokens are concatenated to form
 305 a unified input sequence, which is processed by a Transformer encoder that leverages self-attention
 306 mechanisms to capture inter-modal dependencies. The network outputs optimal joint angle adjust-
 307 ments for precise ball placement control, effectively integrating trajectory information, kinematic
 308 constraints, and strategic objectives within a unified framework.
 309

310 **Training Objective.** To train the model, we employ the mean squared error (MSE) loss function,
 311 which minimizes the discrepancy between the predicted and ground-truth joint adjustments:
 312

$$313 \quad L_{MSE}(\theta') = \frac{1}{N} \sum_{i=1}^N \|\hat{J}_i - J_i\|^2; \text{ where } \hat{J}_i = f_{\theta'}([p_i, v_i, j_i, c_i]). \quad (4)$$

314 Here, $f_{\theta'}$ represents the neural network with parameters θ' , $p_i \in \mathbb{R}^{K \times 3}$ and $v_i \in \mathbb{R}^{K \times 3}$ denote the
 315 ball’s position and velocity history, $j_i \in \mathbb{R}^6$ represents the 6-DOF robot joint configuration, $c_i \in \mathbb{R}^4$
 316 represents the one-hot encoded control signal for the desired landing region, $J_i \in \mathbb{R}^3$ is the ground
 317 truth adjustment vector, and $\hat{J}_i \in \mathbb{R}^3$ is the predicted joint adjustment vector.
 318

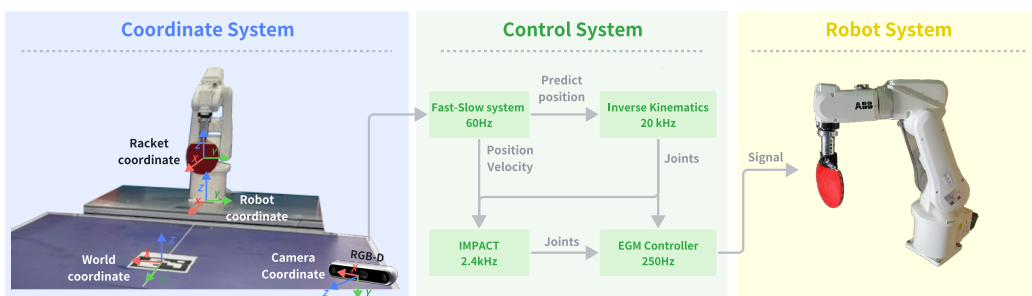
319 Through this imitation learning framework, **IMPACT** enables the robot to dynamically adapt its
 320 striking strategy to varying ball trajectories while precisely targeting specific regions on the oppo-
 321 nent’s court. This capability transforms the system from merely achieving technical accuracy to
 322 executing sophisticated tactical gameplay, significantly enhancing the robot’s strategic competitive-
 323 ness in table tennis matches.
 324

324 4 EXPERIMENTS

326 We present comprehensive evaluations of *SpikePingpong* across multiple dimensions of table tennis
 327 performance. We begin with our experimental setup (Section 4.1), followed by the main results
 328 evaluating contact precision, spatial control, and computational efficiency (Section 4.2). We then
 329 conduct ablation studies to validate our architectural choices (Section 4.3).

331 4.1 EXPERIMENT SETTING

333 **Dataset.** We introduce the *SpikePingpong* Dataset containing two distinct parts for training our
 334 table tennis system. The first part includes 1k samples with trajectory information, expected hit-
 335 table positions, and ground truth deviation vectors collected using RGB-D cameras (60 Hz) and
 336 high-frequency spike cameras (20 kHz). The second part consists of 2k successful return demon-
 337 strations containing ball trajectories, joint configurations, and adjustments for effective returns to
 338 specific court regions. All data were collected using an automated ball launching machine with
 339 randomized trajectories, spins, speeds, and angles under controlled conditions. This comprehen-
 340 sive dataset provides the foundation for training both our trajectory prediction and strategic return
 341 planning components. Detailed information can be found in Appendix D.



351 **Figure 3: System Overview.** Our system integrates three key subsystems: (1) a coordinate system
 352 for spatial tracking and transformation, (2) a multi-frequency control system with Fast-Slow system,
 353 IMPACT, and an EGM controller, and (3) a robot system based on the ABB IRB-120 arm equipped
 354 with a standard table tennis racket.

355 **Implementation Details.** As shown in Fig. 3, our system consists of three integrated subsystems.
 356 The coordinate system handles spatial transformations between world, camera, robot, and racket
 357 coordinates using ArUco marker calibration. The control system operates at multiple frequencies:
 358 Fast-Slow system processes trajectory data at 60Hz and converts predictions to joint configurations
 359 via inverse kinematics at 20kHz, while IMPACT operates at 2.4kHz for striking adjustments with
 360 commands transmitted to the EGM controller at 250Hz. The robot system employs an ABB IRB-
 361 120 robotic arm with a standard table tennis racket, implemented on a workstation with NVIDIA
 362 RTX 4090 GPU. Training details are provided in the Appendix E.

363 **Baselines.** We benchmark against ACT (Zhao et al., 2023) and Diffusion Policy (Chi et al., 2023).
 364 To ensure fair comparison, we optimized both baselines by using state-based inputs (identical to
 365 IMPACT) instead of raw images to eliminate visual latency. Additionally, we accelerated Diffusion
 366 Policy using a 10-step DDIM sampler. All methods employ a synchronous just-in-time one-shot
 367 inference strategy, executing a single forward pass at the latest decision point to leverage the most
 368 accurate state estimation.

370 **Evaluation.** To evaluate our system’s precision and accuracy, we adopt quantitative metrics based
 371 on spatial accuracy. Our evaluation protocol is designed to rigorously assess generalization through
 372 standard offline validation, stochastic online testing, and challenging out-of-distribution scenarios.
 373 First, for ball-racket contact precision (MAE/RMSE), we strictly adhere to standard
 374 machine learning practices by reporting performance on a held-out test set, derived from an 80/10/10
 375 (train/validation/test) split of our collected trajectory dataset. For landing accuracy, we divide the
 376 table tennis court into four regions (A, B, C, D) and measure successful hit rates using two thresholds:
 377 primary accuracy zone (within 30cm of target center) and high precision zone (within 20cm). **Cru-**
 378 **cially, these success rates are evaluated via online physical experiments where the ball launcher gen-**

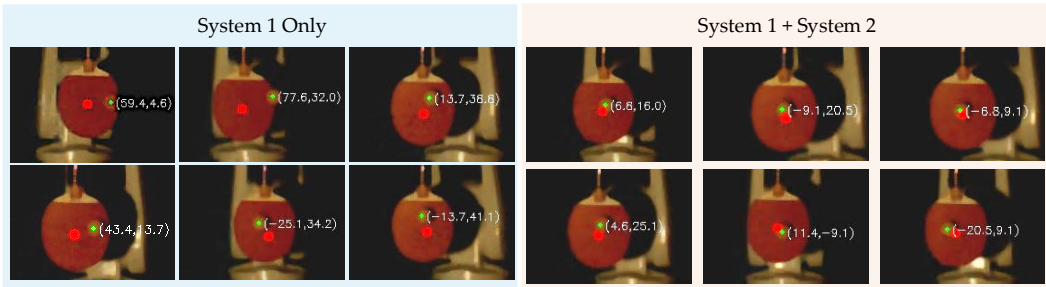


Figure 4: **Visualization of ball-racket contact precision with and without System 2.** Spike-based camera images show the ball center (green) and racket center (red) at contact moment. The reduced offset with Fast-Slow System demonstrates improved ball interception accuracy.

Table 1: **Ball Hittable Position Prediction Error.** Our Fast-Slow system approach achieves superior precision in predicting the actual ball-racket contact point across both axes.

Method	Y-axis		Z-axis		Overall	
	MAE	RMSE	MAE	RMSE	MAE	RMSE
System 1 Only	53.65	60.39	34.62	38.45	44.13	50.62
RNN-based Method (Elman, 1990)	24.10	24.89	21.50	22.52	22.80	23.73
System 1 + System 2	9.87	11.16	14.82	16.10	12.34	13.85

erates completely randomized trajectories (varying spin, speed, and location) for each trial, ensuring the test scenarios are distinct from the training distribution. Furthermore, to assess strong generalization, we conducted Out-of-Distribution (OOD) experiments involving physically relocated launcher positions and zero-shot transfer against unseen human opponents. Due to the absence of publicly available hardware implementations, we rely on these standardized metrics and rigorous controlled validation to demonstrate system performance.

4.2 MAIN RESULTS

Ball-Racket Contact Precision Evaluation Our Fast-Slow system design demonstrated significant improvements in predicting ball-racket contact deviations. Table 1 presents the quantitative results, showing our Fast-Slow system approach achieves superior precision with MAE of 12.34 and RMSE of 13.85 for overall deviation prediction. As shown in Figure 4, it substantially improves contact precision between ball and racket, with spike camera captures revealing minimal separation between ball center (green) and racket center (red), indicating highly accurate interception.

Spatial Control Capabilities We conducted rigorous comparative evaluations against established baseline methods across four strategically positioned target regions (A, B, C, and D). Table 2 presents success rates across various target regions and precision thresholds. *SpikePingpong* exhibits exceptional performance, achieving an average success rate of 92% within the 30cm accuracy zone and 70% within the 20cm high-precision zone, with consistent performance across all target regions. Our system substantially outperforms the human average (53% at 30cm) and all baseline methods. Notably, while baselines like ACT performed better without visual inputs (improving from 12% to 19%), our approach still demonstrates a significant performance leap.

Table 2: **Single-Target Return Accuracy.** Success rates for ball striking across four distinct target regions (A-D) at both 30cm and 20cm precision thresholds. The table compares human players, previous robotic approaches, and our SpikePingpong system. Higher percentages indicate better performance, with all values presented as mean \pm standard deviation.

Method	A		B		C		D		Avg.	
	30cm (%)	20cm (%)								
Human Avg.	48 \pm 6	28 \pm 4	52 \pm 5	32 \pm 3	56 \pm 7	38 \pm 5	54 \pm 4	34 \pm 6	53 \pm 6	33 \pm 5
Diffusion Policy (Chi et al., 2023) (w/ vision)	3 \pm 2	1 \pm 1	4 \pm 3	0 \pm 0	2 \pm 2	1 \pm 1	3 \pm 2	0 \pm 0	3 \pm 2	1 \pm 1
Diffusion Policy (Chi et al., 2023) (w/o vision)	6 \pm 3	7 \pm 2	2 \pm 2	5 \pm 2	1 \pm 1	6 \pm 3	1 \pm 1	6 \pm 3	2 \pm 1	
ACT (Zhao et al., 2023) (w/ vision)	11 \pm 4	4 \pm 2	12 \pm 5	4 \pm 1	10 \pm 3	2 \pm 1	14 \pm 4	5 \pm 2	12 \pm 4	4 \pm 2
ACT (Zhao et al., 2023) (w/o vision)	18 \pm 5	7 \pm 3	20 \pm 6	8 \pm 3	17 \pm 4	6 \pm 2	19 \pm 5	7 \pm 2	19 \pm 5	7 \pm 3
SpikePingpong (Ours)	91 \pm 3	69 \pm 4	93 \pm 2	72 \pm 3	92 \pm 4	70 \pm 5	93 \pm 3	71 \pm 4	92 \pm 3	70 \pm 4

Table 3: **Sequential Target Execution Performance.** Success rates for 100-shot random target sequences. The Success Rate column shows the percentage of individual shots successfully reaching their designated targets (30cm), while subsequent columns present region-specific success rates.

Method	Success Rate(%)	A		B		C		D	
		30cm (%)	20cm (%)						
Human Avg.	45 ± 5	44	26	47	28	43	25	46	29
Diffusion Policy (Chi et al., 2023) (w/ vision)	1 ± 1	1	0	2	0	1	0	1	0
Diffusion Policy (Chi et al., 2023) (w/o vision)	2 ± 2	2	1	3	1	2	0	2	0
ACT (Zhao et al., 2023) (w/ vision)	8 ± 3	7	2	9	3	6	2	10	3
ACT (Zhao et al., 2023) (w/o vision)	15 ± 4	14	5	16	6	13	4	17	5
SpikePingpong (Ours)	78 ± 3	76	52	79	54	77	51	80	55

Sequential Target Execution Capabilities To evaluate our system’s ability to execute tactical sequences, we designed experiments involving random target sequences spanning 100 consecutive returns across four target regions (A, B, C, D), with 25 targets per region presented in random order. We define success using a 30cm precision threshold, with additional 20cm precision metrics provided for detailed analysis. Table 3 presents the results of our sequential target execution experiment. SpikePingpong achieves an overall sequence success rate of 78%, significantly outperforming the human baseline of 45%. Our system demonstrates balanced performance across all court regions with consistent precision under stricter 20cm thresholds. These results demonstrate that our system maintains high precision while executing complex, extended tactical sequences that surpass human-level performance, representing a significant advancement toward sustained strategic gameplay rather than merely returning balls.

Out-of-Distribution Generalization on Robotic Launchers To evaluate the generalization capability of our policy beyond the training distribution, we conducted a challenging out-of-distribution (OOD) experiment. While all training data was collected with the ball launcher at a fixed central position on the opponent’s table, for the OOD test, we physically moved the launcher to two new, unseen off-center positions. This fundamentally altered the entire distribution of incoming ball trajectories, including their angles, speeds, and bounce locations.

As shown in Table 4, while there is a predictable drop in performance compared to the in-distribution setting, our system maintained a remarkable average success rate of 74% for 30cm targets. This result is significant, as the off-center launcher positions create entirely novel trajectories that the policy has never encountered. The sustained high performance strongly suggests that our policy has learned a robust, underlying model of ball dynamics and striking control, rather than simply memorizing patterns from the training data. This validates the generalization capabilities of our framework.

Adaptation and Generalization to Human Demonstrations To push the boundaries of generalization, we tested our system’s ability to adapt to and generalize from complex, human-generated trajectories. Unlike the structured patterns from a robotic launcher, human shots introduce significant, unstructured variability, representing a more challenging data distribution. We conducted a two-stage experiment to assess this capability, with results summarized in Table 5.

First, to test adaptability, we fine-tuned our model on a small dataset of 100 demonstrations from a single human player (Person A). As shown in the "Seen Player" rows of Table 5, when tested on this same player, the system achieved a meaningful success rate of 47% for 30cm targets, demonstrating strong sample efficiency.

Table 5: **Adaptation and Generalization to Human Demonstrations.** Success rates on precision targeting tasks. "Seen Player" refers to testing on the same human demonstrator (Person A) whose data was used for fine-tuning. "Unseen Player" refers to zero-shot testing on a new human player (Person B).

Precision	Condition	A (%)	B (%)	C (%)	D (%)	Avg. (%)
30cm	Seen Player (Person A)	51±5	47±3	42±3	50±4	47±3
	Unseen Player (Person B)	35±6	31±5	27±5	32±4	31±5
20cm	Seen Player (Person A)	29±2	23±4	27±2	28±3	27±3
	Unseen Player (Person B)	18±3	13±4	16±3	14±4	15±4

486
 487 Next, to perform a stricter test of generalization, we evaluated this fine-tuned model in a zero-shot
 488 setting against a new, unseen player (Person B). The results in the "Unseen Player" rows show a
 489 drop in performance to 31%, as expected in a challenging OOD scenario. Nevertheless, achieving
 490 over 31% accuracy on a completely new person without any specific fine-tuning is a non-trivial
 491 result. It provides promising evidence that our model captures generalizable features of human-
 492 like dynamics rather than simply overfitting to an individual's style, highlighting its potential for
 493 collaborative human-robot scenarios.

494 **Computational Efficiency** Real-time responsiveness is
 495 crucial in table tennis robotics. As shown in Table 6,
 496 *SpikePingpong* achieves an inference latency of only
 497 0.407ms, dramatically outpacing Diffusion Policy and
 498 substantially exceeding ACT. This rapid inference capa-
 499 bility provides adequate time for physical actuation, en-
 500 abling responsive gameplay in real-world conditions.

501 4.3 ABLATION STUDY

502 We conducted ablation experiments across four target regions (A, B, C, D) within a 30cm radius
 503 threshold to evaluate each component's contribution. Our Fast-Slow system architecture achieves
 504 92% accuracy in single-target returns, representing a 25-percentage-point improvement over the
 505 RNN (Elman, 1990) baseline. For sequential target execution, our Fast-Slow system achieves 78%
 506 success rate compared to 52% for the RNN-based method (Elman, 1990). This substantial enhance-
 507 ment stems from the system's ability to account for ball-racket interaction sensitivity, where identical
 508 striking motions can produce vastly different trajectories depending on precise contact positioning.
 509 The consistent improvements across both single-target and sequential tasks validate the robustness
 510 of our architectural design.

511 **Table 7: Ablation Study.** Performance comparison of different trajectory prediction components in
 512 our *SpikePingpong* system.

Single-Target Return Accuracy					
Method	A (%)	B (%)	C (%)	D (%)	Avg. (%)
System 1 + IMPACT	22 ± 6	25 ± 5	21 ± 7	24 ± 5	23 ± 6
RNN-based Method (Elman, 1990) + IMPACT	65 ± 5	68 ± 4	66 ± 6	69 ± 3	67 ± 5
Fast-Slow System + IMPACT	91 ± 3	93 ± 2	92 ± 4	93 ± 3	92 ± 3

Sequential Target Execution Performance					
Method	A (%)	B (%)	C (%)	D (%)	Success Rate (%)
System 1 + IMPACT	18 ± 5	20 ± 4	17 ± 6	19 ± 5	15 ± 4
RNN-based Method (Elman, 1990) + IMPACT	55 ± 4	58 ± 5	54 ± 6	57 ± 4	52 ± 6
Fast-Slow System + IMPACT	76 ± 4	79 ± 3	77 ± 4	80 ± 3	78 ± 3

524 5 CONCLUSIONS

525 In this paper, we presented *SpikePingpong*, a high-precision robotic table tennis system integrating
 526 spike vision and advanced control techniques from a cognitive perspective. Our Fast-Slow system
 527 architecture emulates human visual perception processes for enhanced ball detection and trajectory
 528 prediction, while IMPACT handles strategic motion planning for accurate ball striking to specified
 529 target regions. Experiments demonstrate superior performance with 92% success in the primary
 530 accuracy zone and 70% in the high-precision zone, significantly outperforming previous systems.
 531 *SpikePingpong* enables real-time decision-making while executing extended tactical sequences with
 532 a 78% success rate, showcasing sustained strategic gameplay capabilities. The success of our
 533 approach stems from the Fast-Slow architecture that combines rapid physics-based prediction with
 534 neural calibration, and the IMPACT module that enables strategic ball placement through imitation
 535 learning. Beyond table tennis, the core competencies developed in this work, including high-speed
 536 object tracking, precision manipulation, and adaptive control, demonstrate broad applicability to
 537 industrial automation, medical robotics, and aerospace systems. This work advances robotic capa-
 538 bilities in time-critical manipulation tasks requiring precise spatiotemporal coordination.

539 **Table 6: Computational Performance Comparison.** Average inference times
 540 in milliseconds for generating return actions across different methods.

Method	Inference time (ms)
Diffusion Policy (Chi et al., 2023)	25.18
ACT (Zhao et al., 2023)	7.15
<i>SpikePingpong</i>	0.407

540 ETHICS STATEMENT
541542 We acknowledge and adhere to the ICLR Code of Ethics. All data collection focused solely on
543 ball trajectories and paddle movements without storing personally identifiable information. This re-
544 search contributes to recreational robotics applications and presents minimal ethical concerns when
545 developed responsibly.546
547 REPRODUCIBILITY STATEMENT
548549 To ensure the reproducibility of our work, we provide comprehensive implementation details and
550 experimental specifications throughout the paper and supplementary materials. The experimental
551 setup, including hardware specifications, data collection protocols, and evaluation metrics, is thor-
552oughly documented in Appendix B. The dataset collection methodology and preprocessing steps are
553 detailed in Appendix D, enabling replication of our data generation process. Appendix E contains
554 detailed network architectures, hyperparameters, and training procedures for all components of our
555 system. We've provided the code for our method in the supplementary material. Our codebase,
556 including model implementations, training scripts, and evaluation protocols, will be made publicly
557 available upon publication.558
559 REFERENCES
560561 Saminda Wishwajith Abeyruwan, Laura Graesser, David B D'Ambrosio, Avi Singh, Anish Shankar,
562 Alex Bewley, Deepali Jain, Krzysztof Marcin Choromanski, and Pannag R Sanketi. i-sim2real:
563 Reinforcement learning of robotic policies in tight human-robot interaction loops. In *Conference
on Robot Learning*, pp. 212–224. PMLR, 2023.564
565 Leopoldo Acosta, JJ Rodrigo, Juan A Mendez, G Nicolás Marichal, and Marta Sigut. Ping-pong
566 player prototype. *IEEE robotics & automation magazine*, 10(4):44–52, 2003.567 Sonya Alexandrova, Zachary Tatlock, and Maya Cakmak. Roboflow: A flow-based visual program-
568 ming language for mobile manipulation tasks. In *2015 IEEE international conference on robotics
569 and automation (ICRA)*, pp. 5537–5544. IEEE, 2015.570 Luca Anzalone, Paola Barra, Silvio Barra, Aniello Castiglione, and Michele Nappi. An end-to-end
571 curriculum learning approach for autonomous driving scenarios. *IEEE Transactions on Intelligent
572 Transportation Systems*, 23(10):19817–19826, 2022.573
574 Yahav Avigal, Lars Berscheid, Tamim Asfour, Torsten Kröger, and Ken Goldberg. Speedfolding:
575 Learning efficient bimanual folding of garments. In *2022 IEEE/RSJ International Conference on
576 Intelligent Robots and Systems (IROS)*, pp. 1–8. IEEE, 2022.577
578 Amir Hossein Baradaran. Advanced prediction of hypersonic missile trajectories with cnn-lstm-gru
579 architectures. *arXiv preprint arXiv:2506.15043*, 2025.580
581 Qingwei Ben, Feiyu Jia, Jia Zeng, Junting Dong, Dahua Lin, and Jiangmiao Pang.
582 Homie: Humanoid loco-manipulation with isomorphic exoskeleton cockpit. *arXiv preprint
583 arXiv:2502.13013*, 2025.584
585 J. Billingsley. Robot ping pong. *Practical Computing*, 1983.586
587 bubbliiing. yolov4-tiny-pytorch: PyTorch implementation of YOLOv4-tiny. <https://github.com/bubbliiing/yolov4-tiny-pytorch>, 2020.588
589 D. Buchler, S. Guist, R. Calandra, V. Berenz, B. Schölkopf, and J. Peters. Learning to play table
590 tennis from scratch using muscular robots. *IEEE Transactions on Robotics*, 38:3850–3860, Dec.
591 2022. doi: 10.1109/tro.2022.3176207. URL <https://doi.org/10.1109/tro.2022.3176207>.592
593 Dieter Büchler, Simon Guist, Roberto Calandra, Vincent Berenz, Bernhard Schölkopf, and Jan Pe-
594 ters. Learning to play table tennis from scratch using muscular robots. *CoRR*, abs/2006.05935,
595 2020.

594 Cheng Chi, Zhenjia Xu, Siyuan Feng, Eric Cousineau, Yilun Du, Benjamin Burchfiel, Russ Tedrake,
 595 and Shuran Song. Diffusion policy: Visuomotor policy learning via action diffusion. *The International Journal of Robotics Research*, pp. 02783649241273668, 2023.

596

597 David B D'Ambrosio, Jonathan Abelian, Saminda Abeyruwan, Michael Ahn, Alex Bewley, Justin
 598 Boyd, Krzysztof Choromanski, Omar Cortes, Erwin Coumans, Tianli Ding, et al. Robotic table
 599 tennis: A case study into a high speed learning system. *arXiv preprint arXiv:2309.03315*, 2023.

600

601 David B D'Ambrosio, Saminda Abeyruwan, Laura Graesser, Atil Iscen, Heni Ben Amor, Alex Be-
 602 wley, Barney J Reed, Krista Reymann, Leila Takayama, Yuval Tassa, et al. Achieving human
 603 level competitive robot table tennis. In *2025 IEEE International Conference on Robotics and
 604 Automation (ICRA)*, pp. 74–82. IEEE, 2025.

605

606 Rupam Deka, Partha Protim Borthakur, Elora Baruah, Pranjal Sarmah, and Madhurjya Saikia. A
 607 comprehensive review on mechanical conveyor systems: Evolution, types, and applications. *Int.
 608 J. Eng. Nat. Sci.*, 18:164–183, 2024.

609 desigproject. tt2 dataset. <https://universe.roboflow.com/desigproject/tt2-cyt9i>, dec 2022. URL <https://universe.roboflow.com/desigproject/tt2-cyt9i>. visited on 2025-05-12.

610

611

612 Tianli Ding, Laura Graesser, Saminda Abeyruwan, David B D'Ambrosio, Anish Shankar, Pierre
 613 Sermanet, Pannag R Sanketi, and Corey Lynch. Goalseye: Learning high speed precision table
 614 tennis on a physical robot. *arXiv preprint arXiv:2210.03662*, 2022.

615

616 Siwei Dong, Tiejun Huang, and Yonghong Tian. Spike camera and its coding methods. *arXiv
 617 preprint arXiv:2104.04669*, 2021.

618 Jeffrey L Elman. Finding structure in time. *Cognitive science*, 14(2):179–211, 1990.

619

620 Yankai Fu, Qiuixuan Feng, Ning Chen, Zichen Zhou, Mengzhen Liu, Mingdong Wu, Tianxing Chen,
 621 Shanyu Rong, Jiaming Liu, Hao Dong, et al. Cordvip: Correspondence-based visuomotor policy
 622 for dexterous manipulation in real-world. *arXiv preprint arXiv:2502.08449*, 2025.

623

624 Wenbo Gao, Laura Graesser, Krzysztof Choromanski, Xingyou Song, Nevena Lazic, Pannag San-
 625 keti, Vikas Sindhwani, and Navdeep Jaitly. Robotic table tennis with model-free reinforcement
 626 learning. In *IROS*, 2020.

627

628 Xiaoshan Gao, Liang Yan, Zhijun Li, Gang Wang, and I-Ming Chen. Improved deep deterministic
 629 policy gradient for dynamic obstacle avoidance of mobile robot. *IEEE Transactions on Systems,
 Man, and Cybernetics: Systems*, 53(6):3675–3682, 2023.

630

631 Tuomas Haarnoja, Sehoon Ha, Aurick Zhou, Jie Tan, George Tucker, and Sergey Levine. Learning
 632 to walk via deep reinforcement learning. *arXiv preprint arXiv:1812.11103*, 2018.

633

634 Tairan He, Zhengyi Luo, Xialin He, Wenli Xiao, Chong Zhang, Weinan Zhang, Kris Kitani,
 635 Changliu Liu, and Guanya Shi. Omnih2o: Universal and dexterous human-to-humanoid whole-
 636 body teleoperation and learning. *arXiv preprint arXiv:2406.08858*, 2024.

637

638 Tairan He, Jiawei Gao, Wenli Xiao, Yuanhang Zhang, Zi Wang, Jiashun Wang, Zhengyi Luo,
 639 Guanqi He, Nikhil Sobanbabu, Chaoyi Pan, Zeji Yi, Guannan Qu, Kris Kitani, Jessica Hodgins,
 640 Linxi "Jim" Fan, Yuke Zhu, Changliu Liu, and Guanya Shi. Asap: Aligning simulation and real-
 641 world physics for learning agile humanoid whole-body skills. *arXiv preprint arXiv:2502.01143*,
 642 2025.

643

644 Zhe Hu, Yu Zheng, and Jia Pan. Grasping living objects with adversarial behaviors using inverse
 645 reinforcement learning. *IEEE Transactions on Robotics*, 39(2):1151–1163, 2023.

646

647 Binghao Huang, Yuanpei Chen, Tianyu Wang, Yuzhe Qin, Yaodong Yang, Nikolay Atanasov, and
 648 Xiaolong Wang. Dynamic handover: Throw and catch with bimanual hands. *arXiv preprint
 649 arXiv:2309.05655*, 2023.

650

651 Daniel Kahneman. *Thinking, fast and slow*. macmillan, 2011.

648 Seungsu Kim, Ashwini Shukla, and Aude Billard. Catching objects in flight. *IEEE Transactions on*
 649 *Robotics*, 30(5):1049–1065, 2014.
 650

651 Jens Kober, Erhan Öztop, and Jan Peters. Reinforcement learning to adjust robot movements to
 652 new situations. In *IJCAI Proceedings-International Joint Conference on Artificial Intelligence*,
 653 volume 22, pp. 2650. Citeseer, 2011.

654 Fengbo Lan, Shengjie Wang, Yunzhe Zhang, Haotian Xu, Oluwatosin Oseni, Ziye Zhang, Yang
 655 Gao, and Tao Zhang. Dexcatch: Learning to catch arbitrary objects with dexterous hands. *arXiv*
 656 *preprint arXiv:2310.08809*, 2023.
 657

658 Xinyuan Luo, Shengmiao Jin, Hung-Jui Huang, and Wenzhen Yuan. An intelligent robotic sys-
 659 tem for perceptive pancake batter stirring and precise pouring. In *2024 IEEE/RSJ International*
 660 *Conference on Intelligent Robots and Systems (IROS)*, pp. 5970–5977. IEEE, 2024.

661 Hans Moravec. *Mind children: The future of robot and human intelligence*. Harvard University
 662 Press, 1988.
 663

664 Shotaro Mori, Kazutoshi Tanaka, Satoshi Nishikawa, Ryuma Niiyama, and Yasuo Kuniyoshi. High-
 665 speed humanoid robot arm for badminton using pneumatic-electric hybrid actuators. *IEEE*
 666 *Robotics and Automation Letters*, 4(4):3601–3608, 2019.

667 Urs Muller, Jan Ben, Eric Cosatto, Beat Flepp, and Yann Cun. Off-road obstacle avoidance through
 668 end-to-end learning. *Advances in neural information processing systems*, 18, 2005.
 669

670 Katharina Mülling, Jens Kober, and Jan Peters. A biomimetic approach to robot table tennis. In *2010*
 671 *IEEE/RSJ International Conference on Intelligent Robots and Systems*, pp. 1921–1926. IEEE,
 672 2010.

673 Katharina Mülling, Jens Kober, Oliver Kroemer, and Jan Peters. Learning to select and generalize
 674 striking movements in robot table tennis. *The International Journal of Robotics Research*, 32(3):
 675 263–279, 2013.
 676

677 Ramkumar Natarajan, Hanlan Yang, Qintong Xie, Yash Oza, Manash Pratim Das, Fahad Islam,
 678 Muhammad Suhail Saleem, Howie Choset, and Maxim Likhachev. Preprocessing-based kinody-
 679 namic motion planning framework for intercepting projectiles using a robot manipulator. In *2024*
 680 *IEEE International Conference on Robotics and Automation (ICRA)*, pp. 10910–10916. IEEE,
 681 2024.

682 Quan Nguyen, Ayush Agrawal, Xingye Da, William C Martin, Hartmut Geyer, Jessy W Grizzle, and
 683 Koushil Sreenath. Dynamic walking on randomly-varying discrete terrain with one-step preview.
 684 In *Robotics: Science and Systems*, volume 2, pp. 384–99, 2017.
 685

686 Yunpeng Pan, Ching-An Cheng, Kamil Saigol, Keuntaek Lee, Xinyan Yan, Evangelos Theodorou,
 687 and Byron Boots. Agile autonomous driving using end-to-end deep imitation learning. *arXiv*
 688 *preprint arXiv:1709.07174*, 2017.

689 Yunpeng Pan, Ching-An Cheng, Kamil Saigol, Keuntaek Lee, Xinyan Yan, Evangelos A Theodorou,
 690 and Byron Boots. Imitation learning for agile autonomous driving. *The International Journal of*
 691 *Robotics Research*, 39(2-3):286–302, 2020.
 692

693 pingpong. Ping pong detection dataset. <https://universe.roboflow.com/pingpong-ojuhj/ping-pong-detection-0guzq>, may 2024. URL <https://universe.roboflow.com/pingpong-ojuhj/ping-pong-detection-0guzq>.
 694 visited on 2025-05-12.
 695

696 Dean A Pomerleau. Alvinn: An autonomous land vehicle in a neural network. *Advances in neural*
 697 *information processing systems*, 1, 1988.
 698

699 Lin Shao, Fabio Ferreira, Mikael Jorda, Varun Nambiar, Jianlan Luo, Eugen Solowjow, Juan Apari-
 700 cito Ojea, Oussama Khatib, and Jeannette Bohg. Unigrasp: Learning a unified model to grasp with
 701 multifingered robotic hands. *IEEE Robotics and Automation Letters*, 5(2):2286–2293, 2020.

702 Luis Angel Silva, José María Sebastián, R Saltaren, Rafael Aracil, and Jose Sanpedro. Robote-
 703 nis: optimal design of a parallel robot with high performance. In *2005 IEEE/RSJ International*
 704 *Conference on Intelligent Robots and Systems*, pp. 2134–2139. IEEE, 2005.

705 Zhi Su, Bike Zhang, Nima Rahamanian, Yuman Gao, Qiayuan Liao, Caitlin Regan, Koushil Sreenath,
 706 and S Shankar Sastry. Hitter: A humanoid table tennis robot via hierarchical planning and learn-
 707 ing. *arXiv preprint arXiv:2508.21043*, 2025.

708 Kazuma Takada, Midori Kawaguchi, Akira Uehara, Yukiya Nakanishi, Mark Armstrong, Adrien
 709 Verhulst, Kouta Minamizawa, and Shunichi Kasahara. Parallel ping-pong: Exploring parallel
 710 embodiment through multiple bodies by a single user. In *Proceedings of the Augmented Humans*
 711 *International Conference 2022*, pp. 121–130, 2022.

712 Jie Tan, Tingnan Zhang, Erwin Coumans, Atil Iscen, Yunfei Bai, Danijar Hafner, Steven Bohez, and
 713 Vincent Vanhoucke. Sim-to-real: Learning agile locomotion for quadruped robots. *arXiv preprint*
 714 *arXiv:1804.10332*, 2018.

715 Jonas Tebbe, Lukas Krauch, Yapeng Gao, and Andreas Zell. Sample-efficient reinforcement learning
 716 in robotic table tennis. In *ICRA*, 2021.

717 Ashish Vaswani, Noam Shazeer, Niki Parmar, Jakob Uszkoreit, Llion Jones, Aidan N Gomez,
 718 Łukasz Kaiser, and Illia Polosukhin. Attention is all you need. *Advances in neural informa-*
 719 *tion processing systems*, 30, 2017.

720 An Dinh Vuong, Minh Nhat Vu, Hieu Le, Baoru Huang, Huynh Thi Thanh Binh, Thieu Vo, Andreas
 721 Kugi, and Anh Nguyen. Grasp-anything: Large-scale grasp dataset from foundation models.
 722 In *2024 IEEE International Conference on Robotics and Automation (ICRA)*, pp. 14030–14037.
 723 IEEE, 2024.

724 Jack Ng Kok Wah. The rise of robotics and ai-assisted surgery in modern healthcare. *Journal of*
 725 *Robotic Surgery*, 19(1):311, 2025.

726 Yilei Wang and Ling Wang. [retracted] machine vision-based ping pong ball rotation trajectory
 727 tracking algorithm. *Computational Intelligence and Neuroscience*, 2022(1):3835649, 2022.

728 Zhongli Wang, Guohui Tian, and Shijie Guo. Gmm enabled by multimodal information fusion
 729 network for detection and motion planning of robotic liquid pouring. *IEEE Transactions on*
 730 *Neural Networks and Learning Systems*, 2024.

731 Ruihai Wu, Haoran Lu, Yiyan Wang, Yubo Wang, and Hao Dong. Unigarmentmanip: A unified
 732 framework for category-level garment manipulation via dense visual correspondence. In *Pro-*
 733 , pp. 16340–
 734 16350, 2024.

735 Ping Yang, De Xu, Huawei Wang, and Zhengtao Zhang. Control system design for a 5-dof table
 736 tennis robot. In *2010 11th International Conference on Control Automation Robotics & Vision*,
 737 pp. 1731–1735. IEEE, 2010.

738 Andy Zeng, Shuran Song, Johnny Lee, Alberto Rodriguez, and Thomas Funkhouser. Tossingbot:
 739 Learning to throw arbitrary objects with residual physics. *IEEE Transactions on Robotics*, 36(4):
 740 1307–1319, 2020.

741 Chong Zhang, Wenli Xiao, Tairan He, and Guanya Shi. Wococo: Learning whole-body humanoid
 742 control with sequential contacts. *arXiv e-prints*, pp. arXiv–2406, 2024a.

743 Kun Zhang, Zhiqiang Cao, Jianran Liu, Zaojun Fang, and Min Tan. Real-time visual measurement
 744 with opponent hitting behavior for table tennis robot. *IEEE Transactions on Instrumentation and*
 745 *Measurement*, 67(4):811–820, 2018.

746 Yuanhang Zhang, Tianhai Liang, Zhenyang Chen, Yanjie Ze, and Huazhe Xu. Catch it! learning to
 747 catch in flight with mobile dexterous hands. *arXiv preprint arXiv:2409.10319*, 2024b.

748 Tony Z Zhao, Vikash Kumar, Sergey Levine, and Chelsea Finn. Learning fine-grained bimanual
 749 manipulation with low-cost hardware. *arXiv preprint arXiv:2304.13705*, 2023.

756 Zida Zhao, Haodong Huang, Shilong Sun, Jing Jin, and Wenjie Lu. Reinforcement learning for
757 dynamic task execution: A robotic arm for playing table tennis. In *2024 IEEE International*
758 *Conference on Robotics and Biomimetics (ROBIO)*, pp. 608–613. IEEE, 2024.

759

760 Yichao Zhong, Chong Zhang, Tairan He, and Guanya Shi. Bridging adaptivity and safety: Learning
761 agile collision-free locomotion across varied physics. *arXiv preprint arXiv:2501.04276*, 2025.

762

763

764

765

766

767

768

769

770

771

772

773

774

775

776

777

778

779

780

781

782

783

784

785

786

787

788

789

790

791

792

793

794

795

796

797

798

799

800

801

802

803

804

805

806

807

808

809

810
811

A OVERVIEW

812 Due to space limitations, we provide comprehensive implementation details and additional exper-
 813 imental validation in the appendix. Section B presents our complete system architecture, including
 814 the ball launcher, multi-camera vision setup, and robotic execution components. Section C details
 815 our real-time perception pipeline with YOLOv4-tiny ball detection, physics-based filtering, and tra-
 816 jectory prediction. Section D describes our two specialized datasets for the Fast-Slow System and
 817 IMPACT models. Section E provides training specifications. Section F presents extended vali-
 818 dation, including ultra-high precision evaluation and human demonstration integration. Section G
 819 provides a comprehensive failure case analysis to identify system limitations and improvement op-
 820 portunities. Section H discusses current system limitations and outlines future research directions
 821 for enhanced spin modeling, human player adaptability, and strategic gameplay planning. Section I
 822 provides a transparent disclosure of the limited use of Large Language Models in manuscript prepa-
 823 ration. Additionally, we provide supplementary videos demonstrating the robotic system’s real-time
 824 ball-hitting performance and trajectory interception capabilities.

825
826

B SYSTEM OVERVIEW

827 Our system consists of a ball launcher, high-speed camera, depth camera, RGB camera, and robotic
 828 arm, designed to achieve an automated table tennis playing system.

830
831

B.1 BALL LAUNCHING SYSTEM

832 We employ the intelligent table tennis robot PONGBOT NOVA as our ball launching system. This
 833 table-mounted launcher can generate topspin and backspin, with precise landing point control rang-
 834 ing from -2 to +2, and adjustable ball speed between levels 1-3, providing stable and controllable
 835 ball trajectories for our experiments.

837
838

B.2 VISION SYSTEM

839 The vision system comprises three cameras, each dedicated to different tasks:

- 840 • **High-Frequency Camera:** Spike M1K40-H2-Gen3 with a resolution of 1000×1000 and a
 841 maximum frame rate of 20,000 fps. In our experiments, we set a step size of 200, saving
 842 100 images per second, specifically designed to capture the instantaneous contact between
 843 the ball and the paddle, providing high temporal resolution image data for stroke analysis.
- 844 • **Depth Camera:** Intel RealSense D455 with a resolution of 640×480 and a frame rate of
 845 60Hz. This camera is calibrated using ArUco markers and employs YOLO (bubbliliing,
 846 2020) model for ball detection. The system transforms detected pixel coordinates into
 847 world coordinates through intrinsic and extrinsic parameters, enabling real-time tracking
 848 of the ball’s position.
- 849 • **RGB Camera:** Intel RealSense LiDAR Camera L515 with a resolution of 960×540 and a
 850 frame rate of 60Hz. It primarily detects the landing position of the ball after being hit by
 851 the robot, providing feedback for evaluating stroke effectiveness.

852 Figure 5 illustrates the visual comparison between spike camera and conventional RGB camera
 853 captures. Due to its ultra-high frame rate, the spike camera eliminates motion blur entirely, providing
 854 crisp imagery of fast-moving objects that would appear blurred in standard cameras, which is crucial
 855 for precise ball trajectory analysis during high-speed table tennis gameplay.

856
857

B.3 MECHANICAL EXECUTION SYSTEM

858 The execution system utilizes an ABB IRB 120 6 DoF (six-degree-of-freedom) robotic arm with
 859 maximum joint rotation speeds of 250°/s, 250°/s, 250°/s, 320°/s, 320°/s, and 420°/s, respectively.
 860 The arm is equipped with a standard table tennis paddle at its end-effector to execute the optimal
 861 hitting motion calculated by the system.

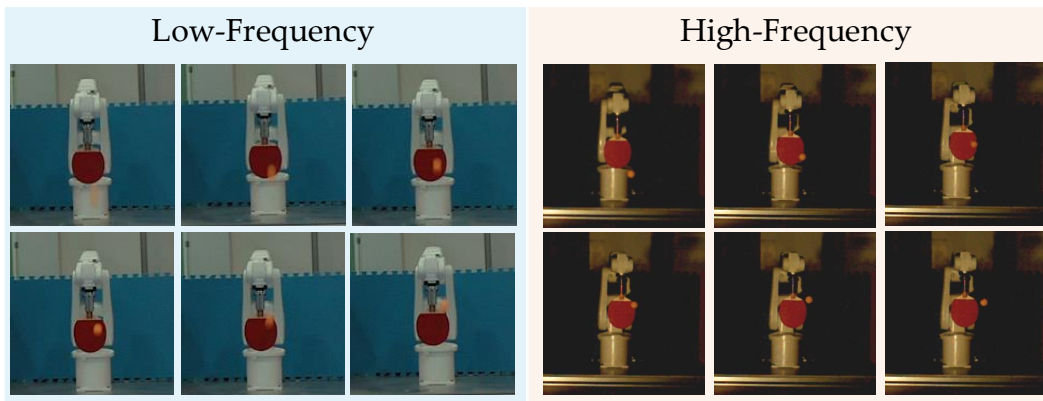


Figure 5: **Comparison of ball capture quality.** Conventional RGB camera with motion blur at 60 fps, Spike camera with crisp imagery at 20,000 fps, demonstrating the advantage of ultra-high frame rate for fast-moving object detection.

This system achieves real-time tracking and precise hitting of table tennis balls through the tight integration of visual perception, trajectory prediction, and motion planning, providing a comprehensive experimental platform for table tennis robotics research.

C DETAILS OF BALL DETECTION AND TRAJECTORY PREDICTION

C.1 BALL DETECTION

In the context of high-speed robotic table tennis, where accurate timing and spatial awareness are critical, a high-frequency vision system is required to continuously track the ball’s position for real-time trajectory estimation and manipulation control. Thus, we chose YOLOv4-tiny (bubbliiing, 2020) due to its lightweight design and computational efficiency, enabling a detection frequency of up to **150 Hz**, which is crucial for the precise and timely interaction with the fast-moving ball. The initial phase of our research involves the supervised training of the detection model using publicly available datasets: Roboflow (Alexandrova et al., 2015), TT2 (desigproject, 2022), and Ping Pong Detection (pingpong, 2024). A two-phase training strategy is implemented to enhance model robustness. In the first phase, the model is trained on the complete dataset. In the second phase, samples that were misdetected during the initial training are selectively sampled and assigned higher weights for fine-tuning, with the goal of improving the detector’s accuracy on difficult instances. Our empirical validation is conducted using an Intel RealSense D455 RGB-D camera, where we employ the optimized lightweight detection model. This setup achieves a detection accuracy that exceeds 99.8%, facilitating rapid and precise 2D positional detection. The results are shown in Figure 6.

C.2 MOTION STATE ESTIMATION FILTER

To accurately track the ball’s motion state, we designed a filtering algorithm that combines physical models with measurement data. This algorithm not only smooths noise in the ball position data but also provides accurate velocity estimates, establishing a foundation for subsequent trajectory prediction and interception planning.

Exponential Moving Average Filter We implemented a physics-based Exponential Moving Average (EMA) filter that simultaneously estimates both position and velocity by combining system dynamics models with real-time observation data. The core formula of the filter is:

$$\hat{x}_t = (1 - \alpha) \cdot f(\hat{x}_{t-1}) + \alpha \cdot z_t \quad (5)$$

where \hat{x}_t is the current state estimate, $f(\hat{x}_{t-1})$ is the dynamics prediction based on the previous state estimate, z_t is the current observation, α is the mixing constant that determines the weight ratio between observation and prediction.

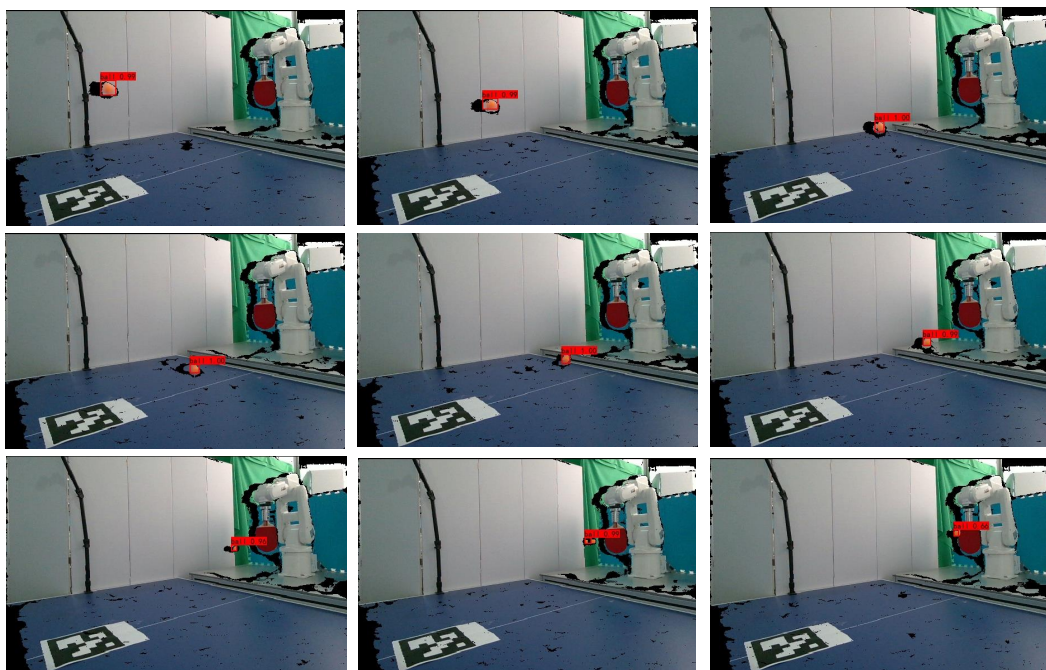


Figure 6: **Visualization of ball detection.** The sequence shows the ball’s trajectory at different time points with accurately placed bounding boxes around the detected ball. Our YOLOv4-tiny model consistently identifies the ball’s position even during high-speed motion, demonstrating the robustness of our detection approach under various lighting conditions and ball velocities.

For the ball’s free-fall motion, we adopted standard ballistic equations as the dynamics model. Specifically, the prediction equations for position and velocity are:

$$\hat{p}_t = \hat{p}_{t-1} + \hat{v}_{t-1} \cdot \Delta t + \frac{1}{2} a \cdot \Delta t^2, \quad (6)$$

$$\hat{v}_t = \hat{v}_{t-1} + a \cdot \Delta t. \quad (7)$$

where, \hat{p}_t is the position estimate, \hat{v}_t is the velocity estimate, Δt is the time step, a is the acceleration (gravity acceleration -9.81 m/s^2 in the z-direction, 0 in x and y directions).

Considering the different motion characteristics of the ball in different directions, we applied different mixing constants for the x, y, and z directions: $\alpha_x = 0.15$, $\alpha_y = 0.15$, $\alpha_z = 0.25$. The larger mixing constant for the z-direction was chosen to better adapt to the faster velocity changes in the vertical direction due to gravity. Additionally, we implemented special handling for the ascending phase in the z-direction to more accurately capture the motion characteristics of the initial segment of the parabolic trajectory.

Implementation Details The system maintains a fixed-length (10 frames) history data queue for calculating initial velocity and handling data interruptions. When a data stream interruption exceeding 1 second is detected, the filter automatically resets the historical data to avoid the influence of outdated information on current estimates. This adaptive mechanism enables the system to quickly resume normal operation when the ball reappears or a new throw begins.

Performance Visualization Experiments show that this filter effectively smooths noise in the raw position data while providing accurate velocity estimates. Since the ball detection algorithm already provides relatively accurate position information, the filter primarily serves to refine and stabilize estimates, particularly excelling in velocity calculation. The filtered trajectory data exhibits smooth parabolic characteristics consistent with physical laws, providing a reliable foundation for subsequent trajectory prediction as shown in Figure 7.

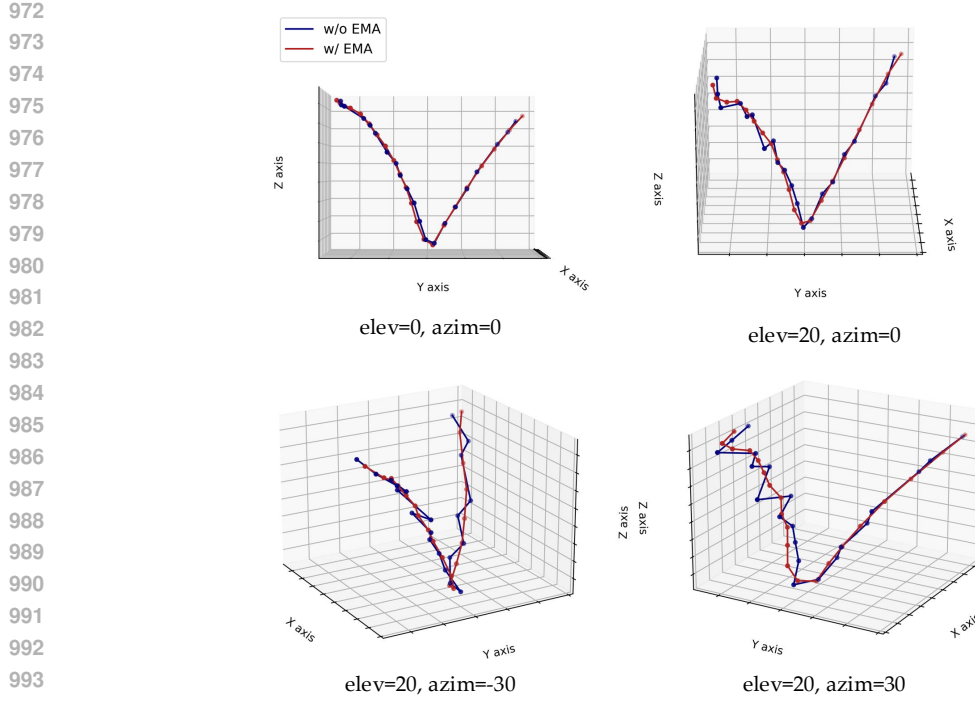


Figure 7: **Comparison of ball trajectory with and without EMA filtering.** The figure displays trajectories from multiple viewing angles, with red curves showing raw detection data and blue curves showing EMA-filtered results. The filtering effectively removes noise while maintaining the ball’s natural parabolic motion, providing more reliable data for trajectory prediction.

C.3 HITTABLE POSITION PREDICTION

To enable the robot to intercept the ball effectively, we developed a trajectory prediction algorithm that estimates where and when the ball will reach a hittable position. This algorithm leverages the filtered position and velocity data from our EMA filter to project the ball’s future path.

Ballistic Model Implementation Our prediction algorithm employs a simplified ballistic model that accounts for gravitational acceleration (9.81 m/s^2), initial position and velocity vectors, and coefficient of restitution for potential bounces. The model deliberately excludes spin effects and complex aerodynamics to maintain computational efficiency and implementation simplicity across both simulation and real-world environments.

Trajectory Prediction The prediction process is implemented using the following Algorithm 1. This algorithm applies the ballistic equations to project the ball’s trajectory forward in time and determine exactly when and where it will intersect the hitting plane. The computed hittable position, impact velocity, and arrival time are then passed to the robot control system for interception planning.

The prediction algorithm includes special handling for various scenarios: trajectories that never intersect the hitting plane, balls moving away from the hitting plane, multiple potential intersections (selecting the earliest valid one), and bounces off other surfaces before reaching the hitting plane.

Integration with Robot Control The predicted hittable position, impact velocity, and arrival time are continuously updated and provided to the robot control system, enabling it to plan and execute appropriate interception movements. This real-time prediction allows the robot to adjust its position and orientation to successfully hit the ball even when the ball follows an unexpected trajectory.

1026 **Algorithm 1** Predict Hittable Position

1027 **Require:** p_0 (initial position), v_0 (initial velocity), $t_{current}$ (current time), y_{plane} (hitting plane

1028 y-coordinate)

1029 **Ensure:** Returns hit position, velocity and arrival time, or null if not hittable

1030 1: $g \leftarrow (0, 0, -9.81)$ Gravity vector

1031 2: **if** $|v_0.y| < \epsilon$ **then**

1032 3: Ball moving parallel to hitting plane

1033 4: **return** null

1034 5: **end if**

1035 6: $t_{hit} \leftarrow (y_{plane} - p_0.y) / v_0.y$

1036 7: **if** $t_{hit} < 0$ **then**

1037 8: Ball already passed the plane

1038 9: **return** null

1039 10: **end if**

1040 11: $p_{hit} \leftarrow p_0 + v_0 \cdot t_{hit} + \frac{1}{2}g \cdot t_{hit}^2$

1041 12: $p_{hit}.y \leftarrow y_{plane}$ Ensure exact y-coordinate

1042 13: $v_{hit} \leftarrow v_0 + g \cdot t_{hit}$

1043 14: $t_{arrival} \leftarrow t_{current} + t_{hit}$

1044 15: **return** $(p_{hit}, v_{hit}, t_{arrival})$

D DATASET DESCRIPTION

This section details the two critical datasets developed for our table tennis robot system. These datasets support the system’s two core components: the Fast-Slow System, focused on precise paddle-contact control, and the IMPACT model (Imitation-based Motion Planning And Control Technology), focused on effective hitting strategies. Below, we describe the collection processes, annotation methods, and how these datasets provide the foundation for the system’s performance.

D.1 DATASET FOR FAST-SLOW SYSTEM

D.1.1 DATA COLLECTION PROCESS

Our data collection process involves the following steps: The ball launcher randomly serves balls within a predetermined range. Based on the Ball Detection and Trajectory Prediction framework described above, we use the Intel RealSense D455 camera to record trajectory information, including position and velocity vectors. Once a hittable position is predicted, this coordinate is transformed into the robotic arm’s base coordinate system. Using PyBullet, we compute the inverse kinematics to determine the joint values required to move to this position, which are then sent to the robotic arm via an EGM Controller. Leveraging the high frame rate capability of the Spike camera, we capture images of the exact moment of contact between the ball and the paddle. This process is repeated multiple times to build a comprehensive dataset.

D.1.2 DATA ANNOTATION PROCESS

Pixel-to-Real-World Conversion A critical step in our data annotation process was establishing an accurate conversion ratio between pixel measurements in images and real-world dimensions. We developed a systematic approach using the known dimensions of the table tennis paddle as a reference.

The process involves the following steps:

1. **Image Acquisition:** We captured multiple high-resolution images of the table tennis paddle using the Spike camera.
2. **Image Preprocessing:** Each image undergoes preprocessing to reduce noise and enhance contrast, facilitating more accurate edge detection. We apply a center-crop operation to focus on the region containing the paddle.

1080 3. **Paddle Detection:** Using color-based segmentation, we isolate the paddle from the back-
 1081 ground by defining a target color range (RGB: 65, 31, 31) with an appropriate tolerance
 1082 value. This creates a binary mask representing the paddle area.
 1083 4. **Morphological Operations:** To refine the mask, we apply morphological operations in-
 1084 cluding opening (to remove small noise artifacts) and closing (to fill small holes), using a
 1085 5×5 kernel.
 1086 5. **Connected Component Analysis:** We identify the largest connected component in the
 1087 mask, which corresponds to the paddle, and filter out smaller noise components.
 1088 6. **Minimum Area Rectangle Fitting:** For the detected paddle region, we compute the min-
 1089 imum area rectangle that encloses the paddle contour, providing us with the paddle's pixel
 1090 dimensions (width and height).
 1091 7. **Conversion Ratio Calculation:** Knowing the actual paddle dimensions (150mm \times
 1092 150mm), we calculate the conversion ratio for both width and height:
 1093

$$\text{mm_per_pixel_width} = \frac{\text{real_width_mm}}{\text{width_pixels}} \quad (8)$$

$$\text{mm_per_pixel_height} = \frac{\text{real_height_mm}}{\text{height_pixels}} \quad (9)$$

1094 8. **Average Conversion Ratio:** To improve accuracy, we average the width and height con-
 1095 version ratios:
 1096

$$\text{mm_per_pixel_avg} = \frac{\text{mm_per_pixel_width} + \text{mm_per_pixel_height}}{2} \quad (10)$$

1097 9. **Multiple Image Processing:** We repeat this process across multiple images and compute
 1098 the overall average conversion ratio to minimize measurement errors.
 1099

1100 This methodology yielded a reliable pixel-to-millimeter conversion factor that was subsequently
 1101 used throughout our data annotation pipeline to transform pixel coordinates in images to real-world
 1102 spatial coordinates.
 1103

1104 D.1.3 BALL-PADDLE CONTACT DETECTION

1105 After establishing the pixel-to-millimeter conversion ratio, we developed a comprehensive algorithm
 1106 to detect and analyze the contact between the table tennis ball and paddle in high-speed scenarios.
 1107 This process is particularly challenging due to the rapid nature of the contact event, which typically
 1108 occurs within milliseconds.
 1109

1110 Our detection pipeline consists of the following key components:
 1111

1112 1. **High Temporal Resolution Acquisition:** The Spike camera captures the ball-paddle inter-
 1113 action with exceptional temporal precision (microsecond-level), providing detailed infor-
 1114 mation about the contact dynamics that conventional cameras would miss. The neuromor-
 1115 phic vision sensor outputs asynchronous spike signals rather than traditional frame-based
 1116 images, enabling ultra-high temporal resolution.
 1117 2. **Ball Detection Strategy:** We implemented a dual-approach ball detection method:
 1118

- 1119 • **Hole-based Detection:** The primary method identifies the ball as a hole or void within
 1120 the paddle region during contact. This approach is particularly effective when the ball
 1121 partially occludes the paddle.
- 1122 • **Color-based Detection:** As a complementary approach, we detect the ball using a
 1123 predefined color range (RGB: 79, 58, 34) with appropriate tolerance values, creating
 1124 a binary mask for potential ball regions.

 1125 3. **Circularity Filtering:** To distinguish the ball from other objects or noise, we apply a
 1126 circularity measure to each detected region:
 1127

$$\text{Circularity} = \frac{4\pi \times \text{Area}}{\text{Perimeter}^2} \quad (11)$$

1128 Regions with circularity above 0.6 are considered potential ball candidates, as table tennis
 1129 balls maintain their circular appearance even during high-speed motion.
 1130

1134 4. **Proximity Analysis:** We prioritize detected ball regions that are within a 20-pixel radius
 1135 of the paddle’s edge, as these are most likely to represent actual contact points.
 1136
 1137 5. **Temporal Sequence Analysis:** By analyzing the sequential spike signals from the neuro-
 1138 morphic camera, we track the ball’s trajectory before, during, and after contact with the
 1139 paddle. This allows us to determine the exact moment of impact with microsecond pre-
 1140 cision.
 1141
 1142 6. **Coordinate System Transformation:** After detecting both the paddle and ball, we estab-
 1143 lish a paddle-centered coordinate system:
 1144 • Origin: Center of the paddle
 1145 • X-axis: Horizontal direction (positive rightward)
 1146 • Y-axis: Vertical direction (positive upward)
 1147
 1148 7. **Contact Point Calculation:** The ball’s position is transformed from pixel coordinates to
 1149 this paddle-centered coordinate system and then converted to physical units (millimeters)
 1150 using our established conversion ratio:
 1151

$$x_{\text{mm}} = (x_{\text{ball}} - x_{\text{paddle}}) \times \text{mm_per_pixel} \quad (12)$$

$$y_{\text{mm}} = (y_{\text{paddle}} - y_{\text{ball}}) \times \text{mm_per_pixel} \quad (13)$$

1153 This ball-paddle contact detection methodology provides unprecedented insights into the dynamics
 1154 of table tennis interactions. By leveraging the unique capabilities of neuromorphic vision sensors,
 1155 we can capture and analyze high-speed interactions that would be impossible to observe with con-
 1156 ventional imaging systems. The resulting data enables quantitative analysis of contact timing, lo-
 1157 cation, and dynamics, which can be valuable for both sports science research and athlete training
 1158 applications.

1160 D.2 DATASET FOR IMPACT

1162 D.2.1 DATA COLLECTION PROCESS

1164 After successfully training the Fast-Slow System to ensure precise ball-paddle contact near the cen-
 1165 ter of the paddle, we extended our data collection to include the hitting phase. Building upon our
 1166 established interception capabilities, we implemented a structured process to collect data on effective
 1167 hitting techniques. For the hitting phase data collection, we augmented our previous methodology
 1168 with the following approach:

1169 1. **Randomized Joint Angle Sampling:** To generate diverse hitting patterns, we implemented
 1170 controlled random sampling on three critical joint axes:
 1171 • Axis 3 (shoulder joint): Base angle of 15.0 degrees with random variation of ± 10.0
 1172 degrees
 1173 • Axis 5 (elbow joint): Base angle of 60.0 degrees with random variation of ± 10.0 degrees
 1174
 1175 • Axis 6 (wrist joint): Base angle of 0 degrees with random variation of ± 20.0 degrees
 1176
 1177 2. **Hitting Execution:** For each trial, the robotic arm would:
 1178 • First, intercept the ball using the Fast-Slow System’s prediction
 1179 • Apply the randomly generated joint angles at the moment of contact
 1180 • Execute the hitting motion to return the ball to the opponent’s side
 1181
 1182 3. **Outcome Recording:** We recorded whether the ball successfully landed on the opponent’s
 1183 side of the table, along with the precise landing location.

1184 This approach allowed us to collect data on effective hitting strategies while leveraging our previ-
 1185 ously established ball interception capabilities. By systematically varying the joint angles during the
 1186 hitting phase, we were able to explore a wide range of possible returns, creating a comprehensive
 1187 dataset that captures the relationship between joint movements and resulting ball trajectories.

1188 D.2.2 DATA ANNOTATION PROCESS
1189

1190 For data annotation, we used an Intel RealSense L515 camera to record the landing position of the
1191 ball. We divided the opponent’s side of the table into four quadrants (labeled A, B, C, and D) and
1192 encoded these landing zones using one-hot encoding. This encoded landing position information
1193 was incorporated as part of the input data, while the randomly sampled joint angles were used
1194 as labels. Using this structured dataset, we employed imitation learning techniques to train our
1195 IMPACT model, enabling it to learn the relationship between desired landing positions and the
1196 required joint movements to achieve them.

1197 E TRAINING DETAILS.
1198

1200 Both System 2 and IMPACT modules were trained for 2000 epochs using the Adam optimizer with
1201 an initial learning rate of 1e-3 and cosine annealing schedule. System 2 used a batch size of 32 with
1202 K=10 consecutive frames as input for trajectory prediction. The IMPACT module employed a batch
1203 size of 4 to handle the complexity of return planning tasks. All positional inputs were normalized
1204 to the range [0,1], while standard scaling was applied to velocity measurements to ensure numerical
1205 stability across varying ball conditions. Training was conducted on a workstation equipped with an
1206 NVIDIA RTX 4090 GPU.

1207 F ADDITIONAL REAL-WORLD EXPERIMENTS
12081209 F.1 ULTRA-HIGH PRECISION EVALUATION
1210

1211 To further validate our system’s precision capabilities and address questions regarding our target
1212 zone selection, we conducted additional experiments using 10cm radius targets following the
1213 methodology of Büchler et al. (Buchler et al., 2022).

1214 **Experimental Setup.** We evaluated our system using 10cm radius target zones across the same
1215 four regions (A, B, C, D) used in our main experiments. This ultra-high precision threshold
1216 represents only 1.5% of the reachable table area, providing an extremely challenging benchmark for
1217 precision assessment.

1218
1219 Table 8: Ultra-high precision evaluation results with 10cm radius targets

Method	A(%)	B(%)	C(%)	D(%)	AVG.(%)
HYSR (Buchler et al., 2022)	-	-	-	-	8
SpikePingpong	31±4	32±3	29±3	35±2	31±3

1220
1221
1222
1223
1224
1225
1226 **Results and Analysis.** Table 8 presents the results of our ultra-high precision evaluation. Our
1227 system achieves an average success rate of 31±3% within the 10cm target zones, substantially out-
1228 performing the 8% success rate reported by Büchler et al. (Buchler et al., 2022) using similar target
1229 specifications.

1230
1231 **Discussion.** These results validate our choice of 20cm and 30cm target zones as meaningful pre-
1232 cision benchmarks while demonstrating that our system maintains reasonable performance even at
1233 ultra-high precision levels. The progressive degradation from 93% (30cm) to 70% (20cm) to 31%
1234 (10cm) reflects the inherent challenges of precise ball placement in table tennis, where even human
1235 players average only 53% success in 30cm zones. Our system’s ability to achieve 31% success in
1236 10cm targets represents a significant advancement in robotic table tennis precision control.

1237 G FAILURE CASE ANALYSIS
1238

1239 To gain deeper insights into our system’s limitations and identify areas for improvement, we con-
1240 ducted a comprehensive failure analysis by categorizing all unsuccessful attempts during our preci-
1241 sion evaluation experiments.

1242

1243

1244

1245

1246

1247

1248

1249

1250

1251

1252

1253

1254

1255

1256

1257

1258

1259

1260

1261

1262

1263

1264

1265

1266

1267

1268

1269

1270

1271

1272

1273

1274

1275

1276

1277

1278

1279

1280

1281

1282

1283

1284

1285

1286

1287

1288

1289

1290

1291

1292

1293

1294

1295

Table 9: Distribution of failure types in precision targeting experiments

Failure Type	Percentage
Ball fails to cross net	4.6%
Correct quadrant, outside 30cm circle	79.1%
Wrong target quadrant	12.5%
Ball fails to land on table	3.8%

Results. Table 9 presents the distribution of failure types observed in our experiments. The analysis reveals that the majority of failures (79.1%) are near-misses where the system correctly identifies the target region but falls short of the required precision threshold.

Analysis and Implications. The failure distribution indicates robust basic control capabilities with specific areas for improvement:

- **Near-miss failures (79.1%):** These cases demonstrate that our system successfully executes the fundamental task of directing the ball toward the intended table region but requires enhanced precision in fine-grained control. This suggests that improvements in trajectory optimization and control parameter tuning could yield significant performance gains.
- **Strategic errors (12.5%):** Wrong quadrant targeting indicates occasional failures in high-level decision making, potentially due to perception errors or planning inconsistencies under challenging conditions.
- **Fundamental control failures (8.4%):** The combined percentage of balls failing to cross the net or land on the table represents basic execution errors, suggesting room for improvement in fundamental trajectory planning and power control.

Root Cause Analysis of Near-Misses. A deeper causal analysis reveals that the prevalence of “near-misses” stems from two primary root causes:

- **Unmodeled Spin Dynamics:** The most significant challenge is unmodeled ball spin. Extreme spin introduces complex aerodynamic effects (the Magnus effect) and alters bounce characteristics in ways our physics-based model does not capture. This can create small but critical, centimeter-level residual errors in our final trajectory prediction, often causing the ball to land just outside the target zone.
- **High Spatio-Temporal Sensitivity:** The task exhibits extreme sensitivity to the precise timing and location of the ball-paddle contact. Even minor variations in the robot’s arrival time at the contact point can subtly alter the impact dynamics and the resulting ball trajectory. This high sensitivity means that even when the overall strategy is correct, slight execution imprecision can lead to a near-miss.

This analysis confirms that our system demonstrates robust basic control with the primary limitation being precision refinement rather than fundamental control failures, providing clear direction for future system enhancements.

H LIMITATIONS AND FUTURE WORK

H.1 CURRENT LIMITATIONS

Despite the achievements demonstrated in this work, our *SpikePingpong* system has several limitations that present opportunities for future enhancement:

Ball Spin Modeling: Our current system does not account for ball spin, which significantly affects optimal interception strategies for different spin types. The Magnus effect and varying bounce characteristics of topspin, backspin, and sidespin balls can lead to trajectory deviations that our physics-based models do not capture.

1296 **Human Player Adaptability:** Performance against human players remains challenging due to the
1297 complex and unpredictable trajectories they generate compared to our controlled training conditions.
1298 Human players exhibit diverse playing styles, strategic variations, and adaptive behaviors that exceed
1299 the scope of our current training data.
1300

1301 H.2 FUTURE RESEARCH DIRECTIONS

1302 Building upon the foundation established by *SpikePingpong*, we identify several promising direc-
1303 tions for future research:
1304

1305 **Spin Dynamics Integration:** Incorporating comprehensive spin modeling into both the Fast-Slow
1306 system architecture and IMPACT module to handle the full spectrum of ball spin effects on trajectory
1307 prediction and strategic planning.
1308

1309 **Adaptive Learning Framework:** Enhancing the system’s adaptability to diverse playing styles
1310 through online learning mechanisms that can adjust to opponent strategies and playing patterns in
1311 real-time.
1312

1313 **Strategic Gameplay Planning:** Developing advanced strategic planning capabilities for human-
1314 robot interaction, including opponent modeling, tactical sequence planning, and adaptive game strat-
1315 egy formulation.
1316

1317 I USE OF LARGE LANGUAGE MODELS

1318 Large Language Models (LLMs) were used in a limited capacity during the preparation of this
1319 manuscript. Specifically, LLMs were employed solely for:
1320

- Grammar correction and proofreading
- Sentence structure improvement and clarity enhancement
- Minor stylistic refinements to improve readability

1325 LLMs were not involved in research ideation, experimental design, data analysis, or the generation
1326 of scientific content. All technical contributions, methodological innovations, experimental results,
1327 and scientific insights presented in this work are entirely the product of the authors’ original research.
1328
1329
1330
1331
1332
1333
1334
1335
1336
1337
1338
1339
1340
1341
1342
1343
1344
1345
1346
1347
1348
1349